Molecular Biology of the Cell
Vol. 18, 4003–4012, October 2007

The Synovial Sarcoma SYT-SSX2 Oncogene Remodels the Cytoskeleton through Activation of the Ephrin Pathway[D]

Roy Barco,* Laura B. Hunt,* Andrea L. Frump,* Christina B. Garcia,* Andrew Benesh,* Robert L. Caldwell,† and Josiane E. Eid*

*Department of Cancer Biology and †Vanderbilt Orthopedic Institute, Vanderbilt University Medical Center, Nashville, TN 37232

Submitted May 25, 2007; Revised July 9, 2007; Accepted July 26, 2007
Monitoring Editor: Mark Ginsberg

Synovial sarcoma is a soft tissue cancer associated with a recurrent t(X:18) translocation that generates one of two fusion proteins, SYT-SSX1 or SYT-SSX2. In this study, we demonstrate that SYT-SSX2 is a unique oncogene. Rather than confer enhanced proliferation on its target cells, SYT-SSX2 instead causes a profound alteration of their architecture. This aberrant morphology included elongation of the cell body and formation of neurite-like extensions. We also observed that cells transduced with SYT-SSX2 often repulsed one another. Notably, cell repulsion is a known component of ephrin signaling. Further analysis of SYT-SSX2–infected cells revealed significant increases in the expression and activation of Eph/ephrin pathway components. On blockade of EphB2 signaling SYT-SSX2 infectants demonstrated significant reversion of the aberrant cytoskeletal phenotype. In addition, we discovered, in parallel, that SYT-SSX2 induced stabilization of the microtubule network accompanied by accumulation of detyrosinated Glu tubulin and nocodazole resistance. Glu tubulin regulation was independent of ephrin signaling. The clinical relevance of these studies was confirmed by abundant expression of both EphB2 and Glu tubulin in SYT-SSX2–positive synovial sarcoma tissues. These results indicate that SYT-SSX2 exerts part of its oncogenic effect by altering cytoskeletal architecture in an Eph-dependent manner and cytoskeletal stability through a concurrent and distinct pathway.

INTRODUCTION

Alteration of cytoskeletal architecture is a frequent feature of cancer cells. It is associated with several key processes of cancer progression such as epithelial-to-mesenchymal transition, cellular migration and invasion, and loss of cell–cell/cell–matrix adhesion (Carthew, 2005; Savagner, 2001; Watanabe *et al.*, 2005; Yamazaki *et al.*, 2005). Tumor cells deregulate their cytoskeletal organization by disrupting signaling pathways that control the homeostasis of cytoskeletal compartments ranging from the actin filament network to the microtubule network and focal adhesion complexes.

One important oncogenic target pathway that converges on the cytoskeleton is the ephrin/Eph system. This pathway involves the interaction between cell-bound ephrin ligands and the Eph receptor tyrosine kinases (RTKs) expressed on neighboring cells. The ephrin family is categorized into two groups, A ligands (ephrin A1–A5) and B ligands (ephrin B1–B3, Pasquale, 2005). The Eph receptors are also subdivided into the EphA class (EphA1–EphA10) and the EphB class (EphB1–EphB6). With only a few exceptions (Pasquale, 2005), ephrin A ligands bind to EphA receptors, whereas ephrin B ligands bind to EphB receptors. One distinctive feature of the ephrin/Eph pathway is that it requires the assembly of large signaling clusters of ligands and receptors for optimal activation (Klein, 2004). In addition, signaling through the ephrin/Eph system can be bidirectional: forward signaling transduced into the Eph-expressing cell and reverse signaling in the ephrin-expressing cell. Signaling through the ephrin/Eph system feeds into numerous downstream pathways, such as the MAP kinase, Jak/Stat, PI3 kinase cascades, and the Rho- or Rac-mediated cytoskeletal pathways (Pasquale, 2005).

The ephrin/Eph system has been classically described as a patterning pathway that regulates cytoarchitecture and determines cell positioning during development and tissue regeneration. These consist of cytoskeleton-dependent events where the ephrins and their receptors shape organs such as the colon (Batlle *et al.*, 2002) and kidney (Ogawa *et al.*, 2006). They were first discovered as the major modulators of axonal guidance, neurite outgrowth, dendritic spine morphogenesis, vasculogenesis, and cellular repulsion (Pasquale, 2005). In addition to these functions, recent work has implicated ephrin signaling in processes important for tumor progression, such as increased tumor angiogenesis (Brantley *et al.*, 2002), enhanced migration (Miao *et al.*, 2000), and loss of adhesion (Zou *et al.*, 1999). The ephrin/Eph pathway is gaining importance in the cancer field because of frequent alterations of its various family members and their inferred involvement in the development of multiple cancers, including breast, colon, brain, lymphoid, malignant melanoma, prostate, and lung cancer (Tang *et al.*, 1999).

Synovial sarcoma is an aggressive soft tissue cancer resistant to current therapies. It is characterized by a t(X;18)(p11;q11) translocation event that juxtaposes the *SYT* (SYnovial sarcoma Translocated) gene on chromosome 18 with an *SSX* gene on the X chromosome (Clark *et al.*, 1994). The resulting

This article was published online ahead of print in *MBC in Press* (http://www.molbiolcell.org/cgi/doi/10.1091/mbc.E07–05–0496) on August 8, 2007.

[D] The online version of this article contains supplemental material at *MBC Online* (http://www.molbiolcell.org).

Address correspondence to: Josiane E. Eid (josiane.eid@vanderbilt.edu).

chimeric product, *SYT-SSX*, generates a fusion protein derived from both genes. The *SYT* component encodes a nuclear protein that interacts with both the SWI/SNF chromatin remodeling complex (Kato *et al.*, 2002) and the p300 acetyltransferase (Eid *et al.*, 2000), suggesting a role in gene regulation. The *SSX* gene belongs to a family of nine members (*SSX1–9*) expressed mostly in germline cells. The vast majority of translocation events in synovial sarcoma involve either *SSX1* or *SSX2* (Ladanyi, 2001). SSX1 and SSX2 are developmental nuclear proteins that associate with polycomb transcription repression complexes and are implicated in the control of gene expression (Lafanechere and Job, 2000). Interestingly, differences in the histology of synovial sarcoma tumors are associated with the particular *SSX* involved in the translocation event (a monophasic spindle cell histology in SYT-SSX2–positive cancers vs. a biphasic histology composed of spindle cells and glandular epithelium in SYT-SSX1–expressing synovial sarcoma; Antonescu *et al.*, 2000).

The t(X;18)(p11;q11) rearrangement is detected in greater than 95% of synovial sarcoma tumors and is thought to play a crucial role in the genesis and progression of this cancer (Clark *et al.*, 1994). Previous studies have revealed that SYT-SSX1 possesses inherent transforming activity (Nagai *et al.*, 2001). SYT-SSX1 transfectants exhibited enhanced proliferation, anchorage-independent growth, and tumorigenicity in nude mice. These properties established SYT-SSX1 as a classic oncogene. The biological effect of SYT-SSX2 on its target cells, however, is still unknown. Uncovering it will therefore be instrumental in understanding the molecular pathogenesis of synovial sarcoma in tumors containing the SYT-SSX2 translocation.

In this study we present evidence that implicates ephrin signaling in this process. Functional experiments to assess the oncogenic role of SYT-SSX2 uncovered a striking cytoskeletal malformation that was controlled by the ephrin/Eph system, specifically through forward signaling mediated by the EphB2 receptor. This perturbed morphology was accompanied by an increase in the stability of the microtubule network and the accumulation of detyrosinated tubulin via a cytoskeletal pathway distinct from ephrin. The SYT-SSX2 oncogene thus appears to function in part by targeting the cytoskeleton in a dual manner.

MATERIALS AND METHODS

Cells and Reagents

NIH3T3 cells were grown in DMEM supplemented with 10% fetal bovine serum (FBS). Antibodies for immunoprecipitation and Western blotting included anti-Ephrin B1 (Zymed, San Francisco, CA), anti-EphA4 (Zymed), anti-EphB2 (Zymed), and anti-pTyr 4G10 (Upstate, Lake Placid, NY). For immunofluorescence studies, anti-hemagglutinin (HA), anti-α-tubulin, and phalloidin, all from Sigma (St. Louis, MO) were used. The following compounds were used for inhibitor treatment of infected cells: PD98069, AG1295, Calphostin C, Go6976, W7, NF0–023, cyclopamine, LY290042, Rac1 inhibitor, SP-600125, Y27632, KT5720, H89, D4476, Genistein, AG1478, SB-20358, SB-220025, U0126, and AG18 all from Calbiochem (La Jolla, CA). KN93 (Biomol, Plymouth Meeting, PA), Compound E (Axxora, San Diego, CA), C3 transferase (Cytoskeleton, Denver, CO), CK1-7 (US Biological, Swampscott, MA), Fugene (Roche, Indianapolis, IN), and pertussis toxin (Sigma) were also used. Chemical treatments were performed overnight, with the exceptions of CK1-7 (4 h) and D4476 (3 h). Concentrations used are indicated in *Results*.

Retroviral Transduction of NIH3T3 Cells

The SYT, SYTdel8, and SYT-SSX2 cDNAs were inserted into the pOZ retroviral construct (a gift from Pat Nakatani, Dana-Farber Cancer Institute, Boston, MA) as previously described (Pretto *et al.*, 2006). Transient retroviral infections were performed as described previously (Pretto *et al.*, 2006) using the phoenix packaging cell system. Viruses were harvested 2 d after transfection and added to NIH3T3 cells for 6 h in the presence of 4 μg/ml polybrene.

Cell Cycle Analysis

For asynchronous cell cycle experiments, cells were collected at 48 and 72 h after infection, fixed at 4°C overnight in ice-cold 70% ethanol, and processed for propidium iodide staining as described (Janumyan *et al.*, 2003). Cell cycle distribution was assessed using a FACSCalibur flow cytometer (BD Biosciences, San Jose, CA) and analyzed by CellQuest software (BD Biosciences).

Bromodeoxyuridine Labeling

Bromodeoxyuridine (BrdU) incorporation assays were performed using the BrdU Incorporation Assay Kit (Roche, Indianapolis, IN) according to the manufacturer's instructions. Briefly, at 48 h after infection, cells on glass coverslips were labeled with BrdU for 60 min and immunostained for incorporation with anti-BrdU antibodies and infection efficiency with anti-HA. The BrdU labeling index was then taken as the ratio of BrdU-positive cells to infected cells.

Apoptosis Assays

Apoptosis was assessed by Annexin V binding as previously described (Janumyan *et al.*, 2003). Induction of apoptosis was examined by using a FACSCalibur flow cytometer (BD Biosciences), and quantitative analysis was carried out using CellQuest software (BD Biosciences).

Microarray Analysis and RT-PCR

Total RNA was extracted from infected NIH3T3 cells using the RNAeasy Miniprep Kit (Qiagen, Valencia, CA) according to the manufacturer's instructions. For microarray experiments, RNA was submitted to the Vanderbilt Microarray Shared Resource Facility for hybridization with Affymetrix Mouse Genome 430a GeneChip arrays. Gene expression intensity of SYT-SSX2 infectants was normalized to the pOZ backbone vector control. For RT-PCR analysis, 1 μg RNA was converted to cDNA using the Superscript II Reverse Transcriptase System (Invitrogen, Carlsbad, CA) according to the manufacturer's instructions. PCR of transcripts was performed using the following primers: EPHRINB1-F: 5′-CCGAAGATTGGAGACAAGCTG-3′; EPHRINB1-R: 5′-GGATCTTGCCCAACCTTCATA-3′; EPHA4R-F: 5′-ATTCCAGATCTGTTCAGGGAG-3′; EPHA4R-R: 5′-ACTGGCTCTCTCTGATGAAGC-3′; EPHB2-F: 5′-ACCTCTACTACTATGAGGCTG-3′; EPHB2-R: 5′-GTTCTCCACAGCCTCGAAGC-3′; GAPDH-F: 5′-CCTTCATTGACCTCAACTAC-3′; and GAPDH-R: 5′-GGAAGGCCATGCCAGTGAGC-3′. The following conditions were used for PCR amplification: 1 cycle of 4 min at 94°C, 32 cycles of 1 min at 94°C, 1 min at 56°C and 1 min at 72°C and 1 cycle of 10 min at 72°C.

Immunoprecipitations

For immunoprecipitations, cells were lysed in RIPA buffer (50 mM Tris, pH 7.5, 150 mM NaCl, 1% deoxycholate, 1% Triton X-100, 0.1% SDS, 1 mM dithiothreitol) for 30 min at 4°C and centrifuged to remove insoluble material. Lysates were incubated with primary antibodies (all at 1 μg/ml final concentration) for 4 h at 4°C. Lysates were then incubated with protein A-Sepharose (Amersham Biosciences, Uppsala, Sweden) for 30 min at 4°C. Immunoprecipitates were then washed in RIPA buffer and boiled in Laemmli sample buffer for Western blot analysis.

Indirect Immunofluorescence

For indirect immunofluorescence studies, cells were plated on coverslips preincubated with 0.2% gelatin in phosphate-buffered saline (PBS). Coverslips were fixed in 3% paraformaldehyde/2% sucrose, washed with PBS, and permeabilized in 0.2% Triton. Cells were washed then blocked for 20 min in 3% goat serum diluted in PBS. Coverslips were incubated with anti-tubulin (1:400) and anti-HA (1:200) antibodies diluted in blocking buffer for 2 h. Coverslips were washed and incubated with Alexa-conjugated secondary antibodies (Molecular Probes, Eugene, OR) for 30 min. Coverslips were washed and mounted on slides using VectaStain with DAPI (Vector Laboratories, Burlingame, CA). For immunostaining of synovial sarcoma tissues, samples were cryosectioned by the Vanderbilt Immunohistochemistry Core and processed for indirect immunofluorescence as described above with the following modifications: the fixation step was performed with ice-cold acetone and primary antibody incubations were performed overnight at 4°C. Cells were visualized using a Zeiss (Axioplan 2) fluorescence microscope (Thornwood, NY).

Ephrin Pathway Blocking Experiments

To perform ephrin pathway blocking experiments, EphB2 monomers were generated from EphB2-Fc dimers (R&D Systems, Minneapolis, MN), respectively. To produce monomers, EphB2-Fc was incubated with Factor Xa protease (0.5 U/μg protein) at 37°C overnight in digestion buffer (150 mM NaCl, 20 mM Tris, pH 8, 2.5 mM $CaCl_2$). Fc fragments and uncleaved protein were removed with a 30-min incubation in protein A-Sepharose (Amersham Biosciences), followed by Factor Xa protease removal using a 30-min incubation in *p*-aminobenzamidine-agarose (Sigma). Monomer production was confirmed by gel electrophoresis/Coomassie staining and quantitated by Lowry assay. Monomers were added to NIH3T3 cells 24 h after infection at a

concentration of 4 μg/ml overnight. Indirect immunofluorescence was then performed as described.

RESULTS

Expression of SYT-SSX2 Results in Perturbation of Cytoskeletal Architecture

To understand the oncogenic function of SYT-SSX2, we began with its impact on cell proliferation. Because synovial sarcoma is a mesenchymal cancer, we chose NIH3T3 cells as the recipient cells where we compared the biological effects of SYT-SSX2 to that of full-length SYT and SYTdl8 (the SYT component in SYT-SSX2). All proteins where transiently expressed in the pOZ retroviral vector as previously described (Pretto *et al.,* 2006) at high efficiency (80–90%; see Figure 1E) and at equivalent levels (Figure 2C).

Contrary to what we expected, we found that ectopic expression of SYT-SSX2 in NIH3T3 cells did not increase proliferation, as measured by both cell counting and BrdU incorporation experiments in the presence of high (Figure 1, A and B) and low serum (data not shown). Rather, upon closer inspection, we noticed a slight but persistent decrease in cell number that corresponded with progressive rounding and detachment of a small subset of SYT-SSX2–expressing cells 48–72 h after infection (Figure 1A). No significant increase in apoptosis (Figure 1C) or accumulation in M-phase (Figure 1D) was detected. This led us to conclude that cell rounding likely reflects a defect in cellular adhesion. Moreover, SYT-SSX2 infectants failed to form colonies in soft agar and were incapable of anchorage-independent growth (data not shown), indicating that SYT-SSX2 biological effects in our system are distinct from those of canonical oncogenes.

Accompanying the adhesion phenotype was an aberrant morphological change that occurred by 48 h after infection in SYT-SSX2–expressing cells. This alteration in morphology included elongation and narrowing of NIH3T3 cells, as well as formation of neurite-like extensions in a significant population of these cells (Figure 2, A, B, and D). We could readily visualize this phenomenon by indirect immunofluorescence with antibodies specific to α-tubulin (Figure 2A). This phenotype is dependent on the chimera-forming addition of SSX2, because SYT and SYTdl8 infectants exhibited normal morphology (Figure 2A). Phalloidin staining demonstrated that F-actin distribution corresponded to the general contour of the microtubule cytoskeleton (Figure 2D). These data suggest that the phenotype represents a general perturbation of normal cytoskeletal organization and results from a dominant effect of the translocation protein.

The formation of these projectile structures could potentially translate into an enhanced migratory phenotype. However, we could not detect an increase in the migration nor invasive capacity of SYT-SSX2 infectants in transwell assays (data not shown), suggesting that this phenomenon does not affect cellular motility in response to a chemokine gradient. It is noteworthy, however, that unlike control vector, SYT and SYTdl8 infectants that were capable of forming normal cell junctions, SYT-SSX2–expressing cells demonstrated a more "scattered" phenotype, carving paths away from each other (Figures 2, A and D, and 3B). This phenomenon reflects an activated positional pathway that results in cell repulsion, without causing a change in the rate of chemotactic migration.

As in NIH3T3 cells, a proliferation defect, an abnormal morphology, and a propensity to detach were consistently observed in different SYT-SSX2–expressing mammalian cell lines, of mesenchymal and epithelial origins (U2-OS; human osteosarcoma, C57MG; murine mammary cell line, and Madin-Darby canine kidney cells [MDCK; data not shown]). This is suggestive of a preserved biological function of SYT-SSX2 across species and cell types.

Taken together, these data confer on SYT-SSX2 unusual oncogenic properties, distinct from those of SYT-SSX1 or other proliferative oncogenes.

Changes in Microtubule Composition and Stability after Ectopic Expression of SYT-SSX2

To ascertain whether the cellular projections emanating from SYT-SSX2 infectants were microtubule-dependent, we treated the cells with a high dosage of nocodazole, a microtubule-destabilizing agent (1 μg/ml; 1 h). To our surprise, we found that SYT-SSX2–expressing cells were highly resistant to the cytoskeletal collapse induced by nocodazole treatment compared with controls (Figure 3A). Nocodazole resistance is generally indicative of a stable microtubular structure enriched in detyrosinated α-tubulin (Glu tubulin; Moreno-Flores *et al.,* 2002). Consistent with a stabilized microtubule network, we detected an elevation of the Glu tubulin species in SYT-SSX2–transduced cells, much of which was localized to the neurite-like extensions (Figure 3, B and C). We then asked whether accumulation of Glu tubulin is augmented in SYT-SSX2–positive synovial sarcoma tumor samples. Four synovial sarcoma samples obtained from patients were confirmed as SYT-SSX–positive by both RT-PCR and SSX2-specific antibody immunostaining (data not shown). Interestingly, all four tumor isolates exhibited pronounced enrichment of Glu tubulin relative to control muscle tissue (Figure 3D). Taken together, these experiments demonstrate that expression of SYT-SSX2 in mesenchymal cells led to active remodeling of not only their cytoskeleton architecture but in its composition as well.

Treatment of Cells with Signaling Pathway Inhibitors Modulates SYT-SSX2–induced Abnormal Morphology

We desired to gain a better understanding of the signal transduction pathway(s) responsible for this cytoskeletal perturbation phenotype, because this could provide us with further insight into the significance of this phenomenon. We tested pharmacological inhibitors of numerous signaling pathways in SYT-SSX2 infectants to determine if abolishment of specific pathways resulted in a reversion of its altered cytoskeleton. We found that inhibition of certain pathways exaggerated the aberrant morphology of SYT-SSX2 infectants, most notable among them was the suppression of the Rho/ROCK pathway (Table 1). This enhanced phenotype was manifested primarily through an increase in the size and number of projections extending from the cell body. Of the inhibitors tested, only the tyrphostin AG18 was capable of completely reverting the phenotype (Figure 4). AG18 is a general inhibitor of tyrosine kinases (Bryckaert *et al.,* 1992), suggesting that tyrosine kinase–mediated cell signaling, such as through a receptor tyrosine kinase, may be involved in the establishment of SYT-SSX2–specific morphology. Because AG18 can effect a multitude of signaling cascades, we were interested in trying to further narrow the list of candidate pathways involved in the cytoskeletal phenotype of SYT-SSX2–expressing cells.

Alteration of the Cytoskeleton in SYT-SSX2 Infectants Is Partially Mediated by Forward Signaling through the EphB2 Receptor

To decipher the underlying pathway(s) causing SYT-SSX2 morphology, we performed Affymetrix microarray analysis on RNA transcripts extracted from cells infected with either SYT-SSX2 cDNA or the control retroviral pOZ backbone.

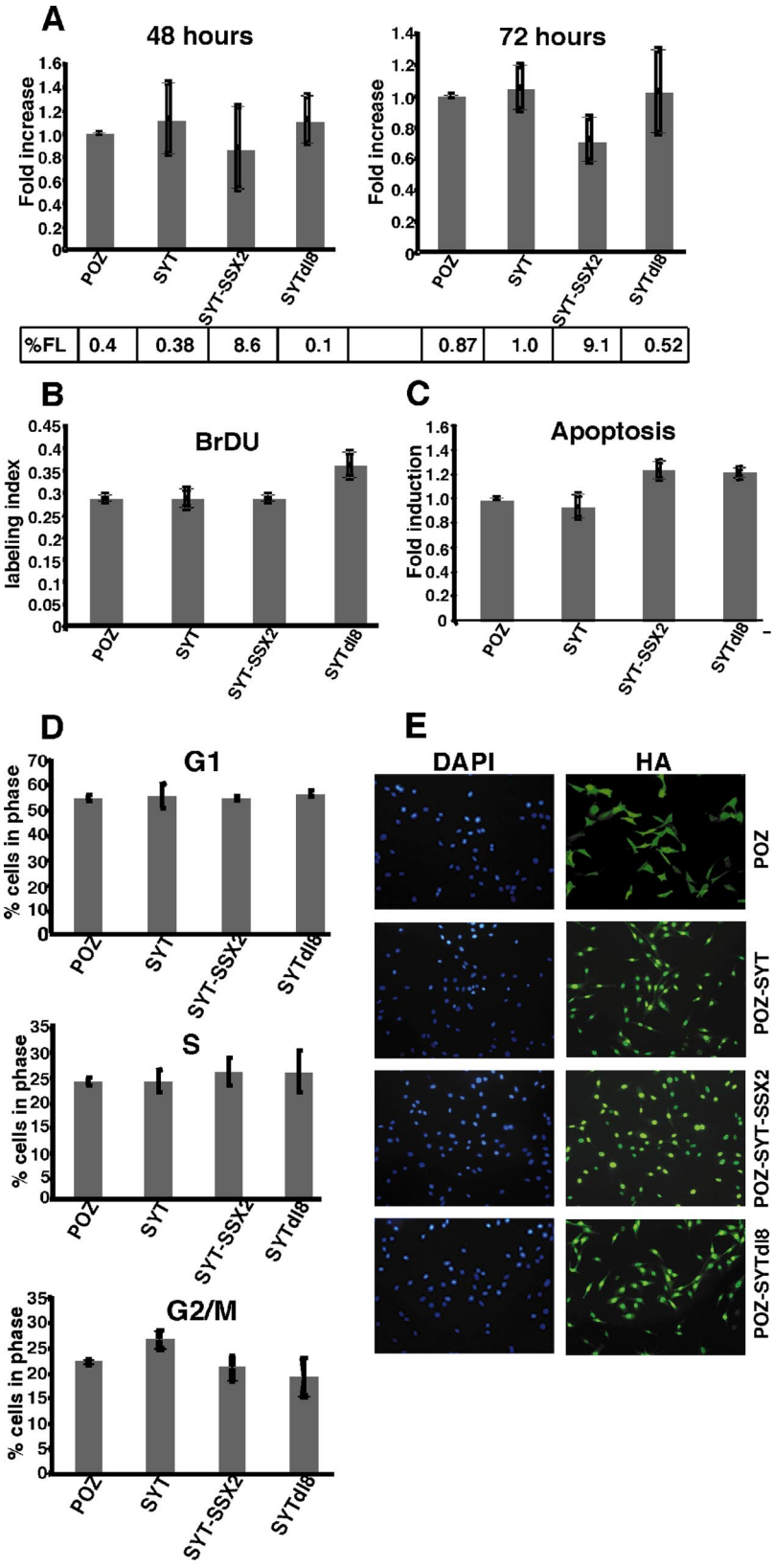

Figure 1. SYT-SSX2 does not alter cellular growth. (A) Proliferation of NIH3T3 cells infected with pOZ, SYT, SYTdel8, and SYT-SSX2 was quantitated by cell counting at 48 and 72 h after infection. Cell counts were normalized to the pOZ retroviral vector control and expressed as fold increase over pOZ. The percentage of floater cells (%FL) detached from the total number of cells in the monolayer was quantitated across conditions and at both time points ($p \leq 0.0025$; $n = 3$). (B) BrdU incorporation in SYT-SSX2–expressing cells and controls, 48 h after infection. Data are represented as a ratio of BrdU-positive cells over total number of infected cells. (C) Apoptosis by annexin V–binding assays in cells transduced with SYT-SSX2 cDNA and controls at 72 h after infection. The percentage of apoptotic cells was normalized to the pOZ retroviral vector and expressed as fold increase over pOZ. (D) Percentage of cells in G1, S, or G2/M in SYT-SSX2 infectants and controls, analyzed by flow cytometry at 72 h after infection. (E) Infection efficiency of the pOZ retroviral transduction system. NIH3T3 cells infected with FLAG/HA-tagged SYT, SYTdel8, SYT-SSX and pOZ retroviral vectors were immunostained with a HA-specific antibody. Left, DAPI stain; right, HA. The cytoplasmic HA staining in pOZ-infected cells is due to the generation of an irrelevant FLAG/HA-tagged peptide by the vector (see Figure 2C). Magnification, 20×.

After hybridization of SYT-SSX2 and pOZ backbone transcripts to microarray platforms, transcript changes were expressed as Log_2 ratios of SYT-SSX2 signal intensity to the pOZ control (where the Log_2 ratio, x, represents twofold increases (or decreases) in transcript level). Gene profiles in SYT-SSX2–expressing cells repeatedly showed changes in the expression patterns of key proteins involved in cell cycle control, signal transduction, cytoskeletal organization, extracellu-

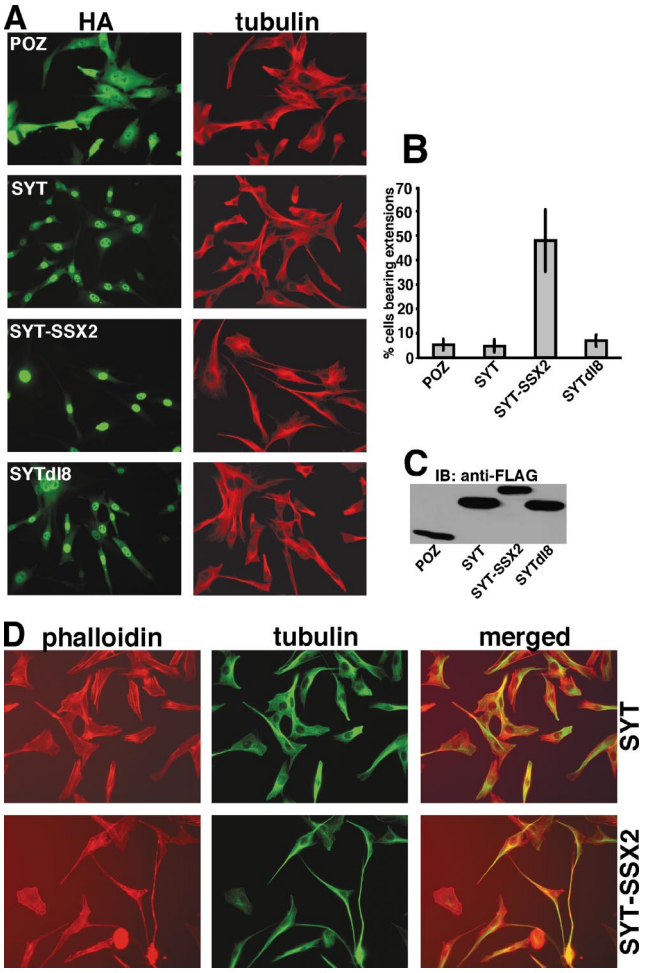

Figure 2. The SYT-SSX2 fusion protein alters the morphology of NIH3T3 cells. NIH3T3 cells were infected with FLAG/HA-tagged pOZ retroviral backbone, pOZ-SYT, pOZ-SYTdel8, and pOZ-SYT-SSX2. (A) Cell body elongation and neurite-like extension formation in SYTSSX2-infected cells. Cells were immunostained for both α-tubulin and HA. Cytoplasmic HA staining in pOZ-infected cells is due to an irrelevant FLAG/HA-tagged peptide (see Figure 2C) generated by the vector and interrupted upon insertion of the SYT and SYT-SSX cDNAs. (B) The percentage of infected cells that produce neurite-like extensions. A total of 1000 cells were counted from fields of equal density (n = 5) and performed in duplicate. (C) Expression levels of pOZ proteins in NIH3T3 cells visualized with the FLAG antibody. (D) SYT and SYT-SSX2 infected cells were double-stained for F-actin (phalloidin) and α-tubulin. A merged image of both immunostains is also shown. An infection rate of >90% in this experiment was confirmed. Magnification, 40×.

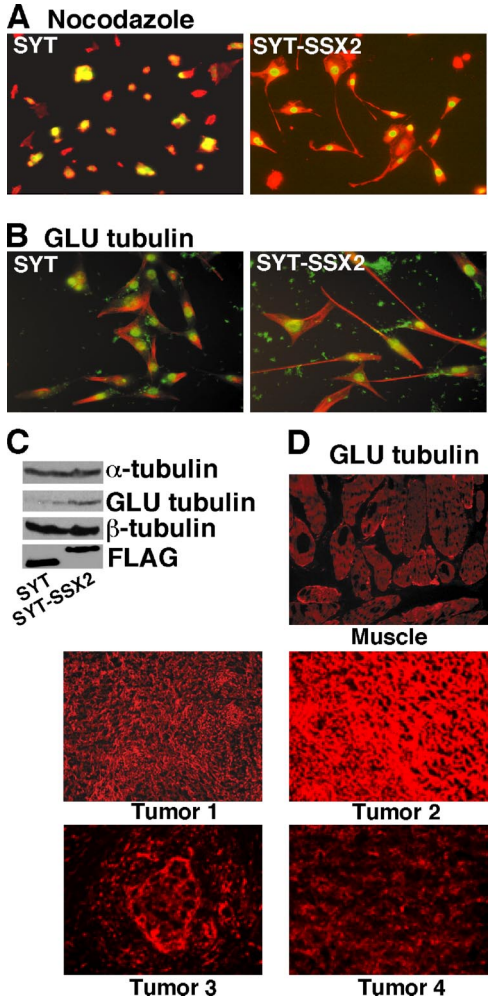

Figure 3. Alteration of microtubule composition in SYT-SSX2 infectants. (A) SYT-SSX2 confers resistance to nocodazole treatment. SYT and SYT-SSX2 infectants were treated with 1 μg/ml nocodazole for 1 h and immunostained with α-tubulin and HA antibodies. Pictures represent merged images of α-tubulin (red) and HA (green). (B) Enrichment of detyrosinated Glu tubulin in SYT-SSX2–expressing cells. Merged images of SYT and SYT-SSX2 infectants immunostained with anti-Glu tubulin (red) and anti-HA (green) antibodies. (A and B) Magnification, 40×. (C) Accumulation of total Glu tubulin in SYT-SSX2 infectants. Levels of α-tubulin, Glu tubulin, β-tubulin, and FLAG-tagged SYT and SYT-SSX2 are shown. (D) Accumulation of Glu tubulin in SYT-SSX2–positive synovial sarcoma tissues. Cryosections of normal muscle control and four synovial sarcoma samples were immunostained with anti-Glu tubulin antibody. Magnification, 20×.

lar matrix components, and transcriptional regulation (Supplementary Tables 1 and 2; GEO Database Accession Nos. GSM180973 and GSM180974). Many corresponded to previously described SYT-SSX targets (e.g., IGF2) or genes known to be differentially expressed in synovial sarcoma (Allander *et al.*, 2002), supporting the validity of our analysis.

One of the most pronounced and reproducible changes observed in our microarray analyses was an increase in the transcript levels of numerous components of the ephrin signaling pathway in SYT-SSX2 infectants; these included the ephrin ligands A3, A4, and B1 as well as the Eph receptors A4, A8, B2, and B3 (Table 2). Multiple hits of at least twofold overexpression in one or both microarray replicates were detected for all of these ephrin pathway members (Table 2). We were intrigued by this pathway for several reasons. First, ephrins regulate numerous processes analogous to the observed phenotype caused by SYT-SSX2. For example, the cellular extensions protruding from SYT-SSX2–transduced cells resemble the neurite outgrowths normally regulated by ephrin signaling (Moreno-Flores *et al.*, 2002). In addition, the "scattered" phenotype of SYT-SSX2 infectants may represent a cellular repulsion event, a process also regulated by ephrin signaling in various cell types (Poliakov *et al.*, 2004). Second, previous microarray studies have detected an overabundance of ephrin ligand and Eph receptor transcripts in synovial sarcoma tumors relative to other soft tissue sarcomas (Nagayama *et al.*, 2002), although it was

Table 1. Effect of signaling inhibitors on SYT-SSX2–induced morphology

Inhibitor	[Conc.]	Pathway affected	Effect	Inhibitor	[Conc.] (μM)	Pathway affected	Effect
DMSO	—	—	None	SP-600125	50	JUNK	None
Pertussis	0.2 μg/ml	GPCR	None	Y27632	10	ROCK I/II	Exaggeration[a]
PD98069	50	MEK1	None	C3 transferase	5 μg/ml	RhoA/B/C	Exaggeration
AG1295	50	PDGF	None	KT5720	5	PKA	Exaggeration
Calphostin C	2.5	PKC	None	H89	25	PKA	Exaggeration
Go6976	200 nM	PKC	None	CK1-7	50	CK1	Exaggeration
W7	30	Calcium	None	D4476	100	CK1	Exaggeration
KN93	10	CAMKII	None	Genistein	10	Tyrosine kinase	Exaggeration
NF-023	50	G-α o/i	None	AG1478	1	EGFR	Exaggeration
Cyclopamine	1	SHH	None	SB-203580	10	p38 MAPK	Exaggeration
Compound E	1	NOTCH	None	SB-220025	10	p38 MAPK	Exaggeration
LY290042	50	PI3K	None	U0126	50	MEK1/2	Partial rescue[a]
Rac inhibitor	50	Rac1	None	AG18	100	Tyrosine kinase	Full rescue

[a] Exaggeration denotes an increase in the number and length of extensions protruding from SYT- SSX2 infectants as well as further narrowing of the cell body rescue.

[b] Partial rescue signifies an incomplete reversion to normal NIH3T3 cell morphology in SYT-SSX2–transduced cells; includes a decrease in the size and number of cellular extensions.

[c] Complete rescue signifies a full reversion to normal NIH3T3 cell morphology in SYT-SSX2 infectants.

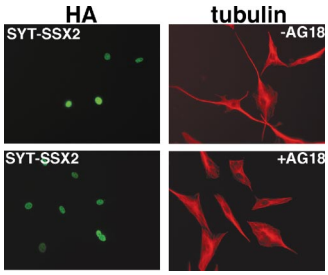

Figure 4. Reversion of SYT-SSX2–induced morphology with the tyrosine kinase inhibitor AG18. SYT-SSX2–infected NIH3T3 cells were treated with either carrier solution (−) or 100 μM AG18 (+) overnight. Cells were visualized by indirect immunofluorescence with α-tubulin (red) and HA (green) antibodies. Magnification, 40×.

Table 2. Eph/ephrin mRNA increases in SYT-SSX2 infectants detected by microarray analysis

		Log_2 increase ratios[a]	
Gene	Accession no.	Microarray hits in replicate 1	Microarray hits in replicate 2
EphA4	BB706548	1.5, 1.5	2.4, 1.9
EphA8	NM_007939.1	—	2.9
EphB2	AV221401	1.8, 1.6	—
EphB3	BC014822.1	1.1	1.1
Ephrin B1	NM_010110.1	3.8, 2.8, 2.5	4.2, 3.2, 2.8
Ephrin A3	AA388313	2.1	2.6
Ephrin A4	NM_007910.1	1.5	1.7

[a] Ratios are of SYT-SSX2 signal intensity over pOZ vector control. —, no microarray hits.

unknown whether this up-regulation played a functional role in synovial sarcoma disease. Finally, the fact that the Eph proteins are receptor tyrosine kinases suggested that they may represent the targets of the AG18-mediated reversion of the SYT-SSX2–specific phenotype. It is therefore possible that increases in ephrin/Eph receptor levels contribute to the cellular morphology and "repulsion" phenotype of SYT-SSX2–expressing cells. We confirmed the changes in ephrin/Eph receptor transcripts detected in our microarray studies using RT-PCR (Figure 5A). In the case of Ephrin B1, EphA4, and EphB2, the transcript increases corresponded to an elevation in protein levels (Figure 5B). We also detected expression of EphB2 in both of our SYT-SSX2–positive monophasic synovial sarcoma tissues (Figure 5D), further implicating EphB2 in the pathogenesis of this disease.

The interaction of ephrin ligand to Eph receptor leads to a receptor clustering process that orients the Eph receptor kinase domains to favor transphosphorylation of the cytoplasmic domains and initiates signaling cascades. These cascades can then be propagated bidirectionally into not only the Eph receptor–expressing cell (forward signaling) but into the ephrin-expressing cell as well (reverse signaling; Pasquale, 2005). Given the overexpression of EphA4, EphB2, and ephrin B1 observed in SYT-SSX2 infectants, we asked whether there was a corresponding change in the phosphorylation status (and thus activation state) of these proteins. Immunoprecipitation of the EphB2 receptor followed by Western blotting with phosphotyrosine-specific antibodies (4G10) revealed an increase in phosphorylated EphB2 (Figure 5C). We were unable to detect phosphorylated ephrin B1 or the EphA4 receptor (data not shown). Enhanced activation of EphB2 is likely the result of both an increase in the receptor level and that of its ligand, ephrin B1 (Figure 5, A and C). The specific hyperphosphorylation of EphB2 demonstrates that forward ephrin signaling, through the EphB2 receptor, is amplified following the ectopic expression of SYT-SSX2.

After the observation of enhanced EphB2 activation in SYT-SSX2–transduced cells, we ascertained whether this pathway contributed to the altered cytoskeleton of these cells. We blocked EphB2 activation using soluble monomers of the extracellular domain of the EphB2 receptor. Soluble EphB2, through competitive interaction with its ephrin B ligands, impairs forward signaling through the EphB2 receptor. Treatment of NIH3T3 cells with soluble EphB2 caused substantial retraction of the SYT-SSX2–induced neurite-like extensions and a profound reduction in their size

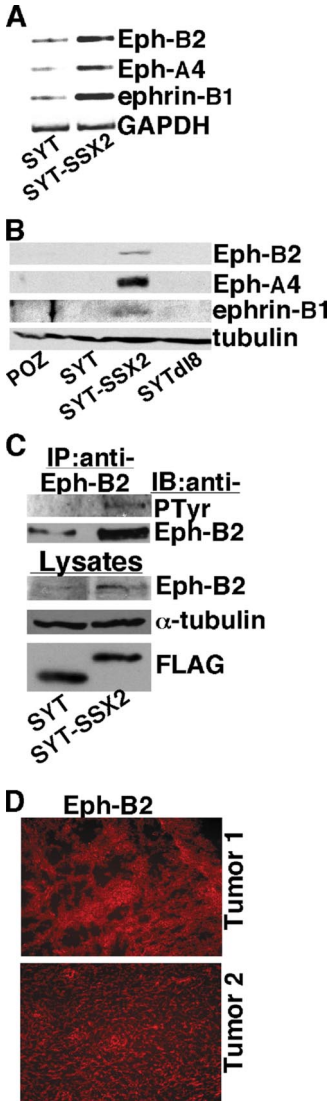

Figure 5. SYT-SSX2 induces an increase in the expression and activation of the EphB2 receptor. (A) Transcript levels of Eph/ephrin pathway components in SYT- and SYT-SSX2–expressing cells examined by RT-PCR. GAPDH cDNA was used as control. (B) Eph/ephrin expression in SYT-SSX2 infectants. NIH3T3 cells infected with pOZ, SYT, SYTdel8, and SYT-SSX2 were immunoblotted with antibodies to EphB2, EphA4, ephrin B1, and α-tubulin as a loading control. (C) Enhanced activation of EphB2 in the presence of SYT-SSX2. Tyrosine-phosphorylated EphB2 was immunoprecipitated from SYT and SYT-SSX2 cell lysates with an EphB2-specific antibody and visualized with anti-pTyr (4G10) antibody. Its identity was confirmed upon reprobing the immunoblot with the EphB2 antibody. Total levels of EphB2 and FLAG-tagged SYT and SYT-SSX2 in the lysates are also indicated with α-tubulin as a loading control. (D) EphB2 expression in cryosections of two SYT-SSX2–positive monophasic synovial sarcoma tumors immunostained with anti-EphB2 antibody. Magnification, 20×.

Figure 6. Rescue of SYT-SSX2–induced cytoskeletal alterations by the blockade of EphB2 forward signaling. (A) Suppression of EphB2 signaling reduces the aberrant morphology of SYT-SSX2–expressing cells. SYT-SSX2 infectants were incubated with either the carrier buffer (−) or with soluble monomeric EphB2 (+) at 4 μg/ml for 18 h. Immunofluorescence using α-tubulin (red) and HA (green) antibodies is displayed as merged images of the both channels. Magnification, 40×. (B) Quantitation of neurite-like extensions after EphB2 signaling blockade. The percentage of cells that bears cellular projections in carrier buffer control and EphB2 monomer–treated SYT-SSX2 infectants was scored from a total of 1000 cells counted from fields of equal density (n = 3) and performed in duplicate.

and number (Figure 6, A and B). It also led to a significant attenuation of the morphological phenotype where the cells lost much of their elongated shape (Figure 6A). In contrast to its effects on the aberrant morphology, we did not observe a suppression of SYT-SSX2–mediated nocodazole resistance and Glu tubulin accumulation after EphB2 monomer treatment (data not shown). This suggests that the enhanced microtubule stability observed in SYT-SSX2 infectants is mediated by a separate pathway that is concurrently activated by the chimeric protein.

Taken together, these data demonstrate an SYT-SSX2–induced alteration of cytoskeletal structure and microtubular composition/stability in NIH3T3 cells.

DISCUSSION

In this study, we have described a novel cytoskeletal phenotype associated with de novo expression of the SYT-SSX2 oncogene. NIH3T3 cells transduced with SYT-SSX2 displayed an alteration of the cytoskeleton that is manifested in the elongation of the cell body as well as the extension of neurite-like processes. The change in cell shape was accompanied by induction of detyrosinated Glu tubulin, the presence of which indicates a stabilized microtubule network.

Mechanistically, activation of the EphB2 forward signaling pathway by SYT-SSX2 contributes significantly to the alteration in morphology caused by this oncogene. Enhanced EphB2 signaling is likely the result of both increases in the EphB2 receptor as well as its interacting ephrin B1 ligand. Microarray and RT-PCR analysis indicated that the induction of EphB2 and its ephrin B1 ligand is most likely mediated at the transcriptional level. Although it is possible that the promoters of these genes may be direct targets for SYT-SSX2, we cannot rule out that these transcript increases are executed through the up-regulation/activation of a master regulator of a cellular program. Regardless of the transcriptional mechanism, the dependence of SYT-SSX2–associated cytoskeletal architecture on EphB2 activation suggests that molecular targeting of the ephrin signaling pathway may be utilized to combat synovial sarcoma.

These in vitro findings reflect important behavioral characteristics of synovial sarcomas. The Ephrin receptor tyrosine kinases (Ephs) are increasingly reputed as proto-oncogenes. This is based on their deregulated activity often observed in numerous cancers (Wimmer-Kleikamp and Lackmann, 2005). Although classical oncogenes upset cell proliferation, differentiation, and apoptotic programs, Ephs instead manipulate cytoskeletal pathways involved in cell positioning and movement. During tumor progression, they are believed to direct and orient cells for metastasis. Moreover, Ephs function in vasculogenesis may induce neovascularization in advanced cancers (Heroult *et al.*, 2006). The striking up-regulation of the ephrin/Eph family members in SYT-SSX2–expressing cells and the resulting aberrant morphology with neurite extensions may illustrate in vivo events occurring in synovial sarcoma formation/progression, whereby Eph activation may position cancer cells for invasiveness and ephrin ligand (ephrin B1) on the surface attract endothelial cells and promote tumor vascularization. Resistance of synovial sarcomas to systemic therapies might be explained by their acquisition of such invasiveness properties early on in tumor development, as soon as the chromosomal rearrangement occurs.

Notably, gene expression profiling in a murine SYT-SSX2 induced synovial sarcomas reiterated the up-regulation of several ephrin/Eph family components (such as EphB2) that we discovered in our NIH3T3 microarray and also reported in several human synovial sarcoma–derived microarrays (Nagayama *et al.*, 2002; Nielsen *et al.*, 2002). These findings reinforce the clinical relevance of ephrin signaling in the context of this cancer. Moreover, the EphB2-mediated elongated shape in SYT-SSX2-NIH3T3 infectants resembles the spindle morphology of human and mouse model-derived monophasic synovial sarcoma, suggesting that this histology is directly attributed to the SYT-SSX2 translocation product.

Although the downstream effectors for this EphB2-mediated cytoskeletal remodeling remain to be characterized, our studies provide preliminary evidence that suppression of Rho signaling may be involved. Inhibitors of both Rho (C3 transferase) and ROCK (Y27632), but not Rac1, caused a pronounced exaggeration of the SYT-SSX2–associated morphology (Table 1). Interestingly, these findings are reminiscent of previous studies that have observed the generation of neurite-like projections after the inhibition of Rho and ROCK in cultured fibroblasts (Scaife *et al.*, 2003). Nonetheless, we cannot rule out other pathways as potential contributors to the cytoskeletal phenotype, such as the ERK pathway, whose inhibition (by U0126) partially reverted this SYT-SSX2–induced morphology. The definitive identity of the effector pathway(s) mediating the Eph-induced phenotype is currently under investigation.

Another potential role for SYT-SSX2 in synovial sarcoma became apparent after the observation that SYT-SSX2–expressing cells were imparted with stable microtubules enriched in detyrosinated Glu tubulin. Immunohistochemistry analysis of SYT-SSX2–expressing synovial sarcoma tumors also demonstrated significant levels of Glu tubulin, corroborating our in vitro cell culture findings. Unlike the morphological changes promoted by SYT-SSX2, the alteration in microtubule composition is not mediated by EphB2 forward signaling. Our microarray analyses suggest that multiple signaling pathways may be concurrently activated in response to SYT-SSX2 expression, one of which likely contributes to the observed microtubule stability. Future studies will be directed toward the elucidation of the pathway responsible for this microtubule phenotype.

The high concentration of Glu tubulin caused by SYT-SSX2 in culture and observed in the synovial sarcoma cryosections could explain in part the aggressive behavior usually associated with this cancer. Glu tubulin is considered a marker of tumor progression and its accumulation frequently heralds poor prognosis for patients affected with several cancers such as human breast cancer, prostate cancer, and neuroblastomas (Kato *et al.*, 2004; Mialhe *et al.*, 2001; Soucek *et al.*, 2006). Accumulation of Glu tubulin has been observed during tumor growth in nude mice (Lafanechere and Job, 2000). How Glu tubulin accumulation specifically contributes to cancer is still largely unknown, although recent studies have implicated it in abnormal spindle positioning (which could lead to genomic instability; Peris *et al.*, 2006) and cellular migration (Gundersen and Bulinski, 1988) and for metastasis induced under hypoxic conditions (Yoon *et al.*, 2005). Another consequence of Glu tubulin enrichment is that it serves as a marker for a stabilized microtubule network that is resistant to microtubule-depolymerizing agents. This notion is consistent with our finding that SYT-SSX2-infectants, containing abundant Glu tubulin, are resistant to high dosages of nocodazole treatment. Although microtubule-depolymerizing agents are often used in cancer chemotherapeutics, this study predicts and cautions that these drugs may possess limited efficacy in synovial sarcoma treatment. Not surprisingly, a recent trial utilizing the microtubule destabilizer vinorelbine in several soft-tissue cancers found no clinical response in synovial sarcoma patients (Casanova *et al.*, 2002).

Our results indicate that SYT-SSX2 and SYT-SSX1 are functionally distinct. Unlike what has been reported with SYT-SSX1 (Nagai *et al.*, 2001), we did not detect proliferative activity or anchorage-independent growth after ectopic expression of SYT-SSX2. This difference may be explained by the nature of the cell line used in our studies (NIH3T3 fibroblasts vs. 3Y1 rat fibroblasts) or the method of ectopic expression (transient retroviral transduction vs. G418-selected stable clones). More likely, there may exist fundamental differences in the functionality of SYT-SSX2 versus SYT-SSX1 (with a 13-amino acids difference in the SSX components) in terms of tumor development. These two chimeric forms may vary in their interaction partners and/or gene targets and thus activate different genetic programs. Distinct gene expression profiles in microarrays derived from SYT-SSX1 (spindle and glandular, biphasic morphology) and SYT-SSX2 (spindle, monophasic morphology) synovial sarcomas (Antonescu *et al.*, 2000) mirror the divergent function and biological effect of the two oncogenes (Fernebro *et al.*, 2005).

Although expression of the SYT-SSX1 fusion is sufficient to promote proliferation and transformation, additional genetic changes (oncogene activation/tumor suppressor inactivation) may be necessary to further expose the oncogenic

potential of SYT-SSX2. This is not surprising, because cooperation between more than one oncogene is frequently required to attain a transformative phenotype (Hanahan and Weinberg, 2000). Nonetheless, SYT-SSX2 could be designated as an oncogene in its own right through its ability to induce the cellular repulsion phenotype reminiscent of Eph-mediated cell positioning seen in numerous tissues. This repulsive effect may manifest itself in vivo as a loss of cell–cell adhesion that initiates the metastatic cascade. Therefore, SYT-SSX2, although not a classical "proliferative oncogene," may function as a "positional oncogene," that, combined with other cancer-promoting events, can generate an aggressive tumor.

The oncogenicity of SYT-SSX2 was recently revealed in a conditional in vivo model where SYT-SSX2 transgenic mice developed tumors that recapitulated synovial sarcomas with 100% penetrance (Haldar *et al.*, 2007). In this model, undifferentiated myogenic progenitors were the prime SYT-SSX2 targets for tumor formation, reinforcing the notion that human synovial sarcomas originate in mesenchymal progenitor/stem cells.

Taken together, these studies describe a novel function for the SYT-SSX2 fusion protein in the alteration of cellular architecture and cytoskeletal composition. A complete understanding of this SYT-SSX2–induced cytoskeletal remodeling and the pathways that contribute to it could ultimately be exploited as a therapeutic tool against synovial sarcoma.

ACKNOWLEDGMENTS

We thank Dr. Lynn Matrisian for critical analysis of this manuscript. This work was supported by Grant RO1CA106481-01 and by the Public Health Service award T32 GM07347 from the National Institute of General Medical Studies for the Vanderbilt Medical-Scientist Training Program.

REFERENCES

Allander, S. V., Illei, P. B., Chen, Y., Antonescu, C. R., Bittner, M., Ladanyi, M., and Meltzer, P. S. (2002). Expression profiling of synovial sarcoma by cDNA microarrays: association of ERBB2, IGFBP2, and ELF3 with epithelial differentiation. Am. J. Pathol. *161*(5), 1587–1595.

Antonescu, C. R., Kawai, A., Leung, D. H., Lonardo, F., Woodruff, J. M., Healey, J. H., and Ladanyi, M. (2000). Strong association of SYT-SSX fusion type and morphologic epithelial differentiation in synovial sarcoma. Diagn. Mol. Pathol. *9*(1), 1–8.

Batlle, E. *et al.* (2002). Beta-catenin and TCF mediate cell positioning in the intestinal epithelium by controlling the expression of EphB/ephrinB. Cell *111*(2), 251–263.

Brantley, D. M. *et al.* (2002). Soluble Eph A receptors inhibit tumor angiogenesis and progression in vivo. Oncogene *21*(46), 7011–7026.

Bryckaert, M. C., Eldor, A., Fontenay, M., Gazit, A., Osherov, N., Gilon, C., Levitzki, A., and Tobelem, G. (1992). Inhibition of platelet-derived growth factor-induced mitogenesis and tyrosine kinase activity in cultured bone marrow fibroblasts by tyrphostins. Exp. Cell Res. *199*(2), 255–261.

Carthew, R. W. (2005). Adhesion proteins and the control of cell shape. Curr. Opin. Genet. Dev. *15*(4), 358–363.

Casanova, M., Ferrari, A., Spreafico, F., Terenziani, M., Massimino, M., Luksch, R., Cefalo, G., Polastri, D., Marcon, I., and Bellani, F. F. (2002). Vinorelbine in previously treated advanced childhood sarcomas: evidence of activity in rhabdomyosarcoma. Cancer *94*(12), 3263–3268.

Clark, J., Rocques, P. J., Crew, A. J., Gill, S., Shipley, J., Chan, A. M., Gusterson, B. A., and Cooper, C. S. (1994). Identification of novel genes, SYT and SSX, involved in the t(X;18)(p11.2;q11.2) translocation found in human synovial sarcoma. Nat. Genet. *7*(4), 502–508.

Eid, J. E., Kung, A. L., Scully, R., and Livingston, D. M. (2000). p300 interacts with the nuclear proto-oncoprotein SYT as part of the active control of cell adhesion. Cell *102*(6), 839–848.

Fernebro, J. *et al.* (2005). Gene expression profiles relate to SS18/SSX fusion type in synovial sarcoma. Int. J. Cancer *118*(5), 1165–1172.

Gundersen, G. G., and Bulinski, J. C. (1988). Selective stabilization of microtubules oriented toward the direction of cell migration. Proc. Natl. Acad. Sci. USA *85*(16), 5946–5950.

Haldar, M., Hancock, J. D., Coffin, C. M., Lessnick, S. L., and Capecchi, M. (2007). A conditional mouse model of synovial sarcoma: insights into a myogenic origin. Cancer Cell *11*, 375–388.

Hanahan, D., and Weinberg, R. A. (2000). The hallmarks of cancer. Cell *100*(1), 57–70.

Heroult, M., Schaffner, F., and Augustin, H. G. (2006). Eph receptor and ephrin ligand-mediated interactions during angiogenesis and tumor progression. Exp. Cell Res. *312*, 642–650.

Janumyan, Y. M., Sansam, C. G., Chattopadhyay, A., Cheng, N., Soucie, E. L., Penn, L. Z., Andrews, D., Knudson, C. M., and Yang, E. (2003). Bcl-xL/Bcl-2 coordinately regulates apoptosis, cell cycle arrest and cell cycle entry. EMBO J. *22*(20), 5459–5470.

Kato, C., Miyazaki, K., Nakagawa, A., Ohira, M., Nakamura, Y., Ozaki, T., Imai, T., and Nakagawara, A. (2004). Low expression of human tubulin tyrosine ligase and suppressed tubulin tyrosination/detyrosination cycle are associated with impaired neuronal differentiation in neuroblastomas with poor prognosis. Int. J. Cancer *112*(3), 365–375.

Kato, H. *et al.* (2002). SYT associates with human SNF/SWI complexes and the C-terminal region of its fusion partner SSX1 targets histones. J. Biol. Chem. *277*(7), 5498–5505.

Klein, R. (2004). Eph/ephrin signaling in morphogenesis, neural development and plasticity. Curr. Opin. Cell Biol. *16*(5), 580–589.

Ladanyi, M. (2001). Fusions of the SYT and SSX genes in synovial sarcoma. Oncogene *20*(40), 5755–5762.

Lafanechere, L., and Job, D. (2000). The third tubulin pool. Neurochem. Res. *25*(1), 11–18.

Mialhe, A. *et al.* (2001). Tubulin detyrosination is frequent occurrence in breast cancers of poor prognosis. Cancer Res. *61*(13), 5024–7.

Miao, H., Burnett, E., Kinch, M., Simon, E., and Wang, B. (2000). Activation of EphA2 kinase suppresses integrin function and causes focal-adhesion-kinase dephosphorylation. Nat. Cell Biol. *2*(2), 62–69.

Moreno-Flores, M. T., Martin-Aparicio, E., Avila, J., Diaz-Nido, J., and Wandosell, F. (2002). Ephrin-B1 promotes dendrite outgrowth on cerebellar granule neurons. Mol. Cell Neurosci. *20*(3), 429–446.

Nagai, M. *et al.* (2001). Analysis of transforming activity of human synovial sarcoma-associated chimeric protein SYT-SSX1 bound to chromatin remodeling factor hBRM/hSNF2 alpha. Proc. Natl. Acad. Sci. USA *98*(7), 3843–3848.

Nagayama, S. *et al.* (2002). Genome-wide analysis of gene expression in synovial sarcomas using a cDNA microarray. Cancer Res. *62*(20), 5859–5866.

Nielsen, T. O. *et al.* (2002). Molecular characterization of soft tissue tumors: a gene expression study. Lancet *359*(9314), 1301–1307.

Ogawa, K., Wada, H., Okada, N., Harada, I., Nakajima, T., Pasquale, E. B., and Tsuyama, S. (2006). EphB2 and ephrin-B1 expressed in the adult kidney regulate the cytoarchitecture of medullary tubule cells through Rho family GTPases. J. Cell Sci. *119*(Pt3), 559–570.

Pasquale, E. B. (2005). Eph receptor signalling casts a wide net on cell behaviour. Nat. Rev. Mol. Cell Biol. *6*(6), 462–475.

Peris, L. *et al.* (2006). Tubulin tyrosination is a major factor affecting the recruitment of CAP-Gly proteins at microtubule plus ends. J. Cell Biol. *174*(6), 839–849.

Poliakov, A., Cotrina, M., and Wilkinson, D. G. (2004). Diverse roles of eph receptors and ephrins in the regulation of cell migration and tissue assembly. Dev. Cell *7*(4), 465–480.

Pretto, D., Barco, R., Rivera, J., Neel, N., Gustavson, M. D., and Eid, J. E. (2006). The synovial sarcoma translocation protein SYT-SSX2 recruits beta-catenin to the nucleus and associates with it in an active complex. Oncogene *25*(26), 3661–3669.

Savagner, P. (2001). Leaving the neighborhood: molecular mechanisms involved during epithelial-mesenchymal transition. Bioessays *23*(10), 912–923.

Scaife, R. M., Job, D., and Langdon, W. Y. (2003). Rapid microtubule-dependent induction of neurite-like extensions in NIH3T3 fibroblasts by inhibition of ROCK and Cbl. Mol. Biol. Cell *14*(11), 4605–4617.

Soucek, K., Kamaid, A., Phung, A. D., Kubala, L., Bulinski, J. C., Harper, R. W., and Eiserich, J. P. (2006). Normal and prostate cancer cells display distinct molecular profiles of alpha-tubulin posttranslational modifications. Prostate *66*(9), 954–965.

Tang, X. X., Brodeur, G. M., Campling, B. G., and Ikegaki, N. (1999). Coexpression of transcripts encoding EPHB receptor protein tyrosine kinases and their ephrin-B ligands in human small cell lung carcinoma. Clin. Cancer Res. *5*(2), 455–460.

Watanabe, T., Noritake, J., and Kaibuchi, K. (2005). Regulation of microtubules in cell migration. Trends Cell Biol. *15*(2), 76–83.

Wimmer-Kleikamp, S. H., and Lackmann, M. (2005). Eph-modulated cell morphology, adhesion and motility in carcinogenesis. IUBMB Life *57*(6), 421–431.

Yamazaki, D., Kurisu, S., and Takenawa, T. (2005). Regulation of cancer cell motility through actin reorganization. Cancer Sci. *96*(7), 379–386.

Yoon, S. O., Shin, S., and Mercurio, A. M. (2005). Hypoxia stimulates carcinoma invasion by stabilizing microtubules and promoting the Rab11 trafficking of the alpha6beta4 integrin. Cancer Res. *65*(7), 2761–2769.

Zou, J. X., Wang, B., Kalo, M. S., Zisch, A. H., Pasquale, E. B., and Ruoslahti, E. (1999). An Eph receptor regulates integrin activity through R-Ras. Proc. Natl. Acad. Sci. USA *96*(24), 13813–13818.